Climate Dynamics (2004) 22: 823–838
DOI 10.1007/s00382-004-0413-1

K. Braganza · D. J. Karoly · A. C. Hirst · P. Stott
R. J. Stouffer · S. F. B. Tett

Simple indices of global climate variability and change Part II: attribution of climate change during the twentieth century

Received: 27 May 2003 / Accepted: 26 January 2004 / Published online: 19 May 2004

Abstract Five simple indices of surface temperature are used to investigate the influence of anthropogenic and natural (solar irradiance and volcanic aerosol) forcing on observed climate change during the twentieth century. These indices are based on spatial fingerprints of climate change and include the global-mean surface temperature, the land-ocean temperature contrast, the magnitude of the annual cycle in surface temperature over land, the Northern Hemisphere meridional temperature gradient and the hemispheric temperature contrast. The indices contain information independent of variations in global-mean temperature for unforced climate variations and hence, considered collectively, they are more useful in an attribution study than global mean surface temperature alone. Observed linear trends over 1950–1999 in all the indices except the hemispheric temperature contrast are significantly larger than simulated changes due to internal variability or natural (solar and volcanic aerosol) forcings and are consistent with simulated changes due to anthropogenic (greenhouse gas and sulfate aerosol) forcing. The combined, relative influence of these different forcings on observed trends during the twentieth century is investigated using linear regression of the observed and simulated responses of the indices. It is found that anthropogenic forcing accounts for almost all of the observed changes in surface temperature during 1946–1995. We found that early twentieth century changes (1896–1945) in global mean temperature can be explained by a combination of anthropogenic and natural forcing, as well as internal climate variability. Estimates of 'scaling factors' that weight the amplitude of model simulated signals to corresponding observed changes using a combined normalized index are similar to those calculated using more complex, optimal fingerprint techniques.

K. Braganza (✉) · D. J. Karoly
School of Mathematics Sciences, Monash University,
PO Box 28M, Clayton, VIC 3800, Australia
E-mail: Karl.Braganza@sci.monash.edu.au

A. C. Hirst
CSIRO Atmospheric Research, Aspendale, VIC, Australia

P. Stott · S. F. B. Tett
Hadley Center for Climate Prediction and Research,
Meteorological Office, Bracknell, Berks., UK

R. J. Stouffer
Geophysical Fluid Dynamics Laboratory, Princeton, NJ, USA

Present address: D. J. Karoly
School of Meteorology, University of Oklahoma,
Norman, OK, USA

1 Introduction

In Part 1 of this study (Braganza et al. 2003), five simple indices of area-average surface temperature were used to describe global-scale climate variability in observations and several global climate model (GCM) control simulations. These indices were the global-mean temperature, mean land-ocean temperature contrast, mean magnitude of the annual cycle in temperature over land, the meridional temperature gradient in the Northern Hemisphere mid-latitudes and the Northern Hemisphere-Southern Hemisphere temperature contrast. On interannual and decadal time scales, it was shown that the covariance structure of the indices was generally similar in long control climate simulations, detrended observations during the twentieth century and proxy based climate reconstructions for the period 1700–1900. In addition, the observed correlation structure between the indices during the twentieth century on decadal time scales showed significant differences to the control simulations and detrended observations. These differences were found to be similar to anthropogenic forced climate change simulations.

While it was suggested that changes to the index-correlation structure can be used as an indicator of radiative forced climate change, an evaluation of any such signal is better served by investigating the time-

dependent evolution of the indices over the past century. In a similar manner to Karoly and Braganza (2001), the purpose of this work is to compare observed temporal changes in the indices during the twentieth century with model simulations of forced and unforced climate. Whereas Karoly and Braganza (2001) examined only the mean magnitude of linear trends from only two GCMs, we greatly expand upon this work by including three more climate models and model experiments including anthropogenic (greenhouse gas and sulfate aerosol) as well as *natural* (solar irradiance and volcanic aerosol) forcing changes. In addition, we also analyse the recent time-dependent response in the indices to discriminate between these two forcings. We follow the approach of several recent optimal fingerprint detection studies (Hegerl et al. 1997; Stott et al. 2000a, b, 2001; Tett et al. 1999, 2002) and use linear regression techniques to compare the amplitude of the forced response in the indices with observed changes. This technique is applied to each of the five surface temperature indices separately as well as to a single combined index of climate change.

2 Data sets

The data used here are the same as those analysed in Braganza et al. (2003). In addition to control and anthropogenic climate change simulations from five coupled ocean-atmosphere climate models, we also make use of experiments using variations of natural forcing.

2.1 Observations

A 5° global grid of blended surface air temperature anomalies over land and sea surface temperature anomalies (Jones et al. 1999) is used. These data are obtained from quality controlled instrumental observations and have been used in a majority of recent studies in climate change. As in Braganza et al. (2003), these data are used for the period 1880–1999, with the period prior to 1880 excluded due to sparse coverage.

2.2 Climate model data

2.2.1 Global climate models

Near-surface air temperature data from five coupled ocean-atmosphere climate models are included in this analysis. Each of the models was also used in the IPCC TAR (McAvaney et al. 2001). Very brief descriptions of the models are given.

The Geophysical Fluid Dynamics Laboratory GCM (GFDL R30) A spectral atmospheric model with rhomboidal truncation at wave number 30 equivalent to 3.75° longitude × 2.2° latitude (96 × 80) with 14 levels in the vertical. The atmospheric model is coupled to an 18 level gridpoint (192 × 80) ocean model where two ocean grid boxes under-lie each atmospheric grid box exactly. Both models are described by Delworth et al. (2002) and Dixon et al. (2002).

The CSIRO Mark 2 GCM (CSIRO Mk2) An atmospheric R21 spectral model with an equivalent horizontal resolution 5.6° longitude × 3.2° latitude (64 × 56) and 9 levels in the vertical. This is coupled to a gridpoint ocean model of the same horizontal resolution with 21 vertical levels (Gordon and O'Farrell 1997; Hirst et al. 2000).

The Hadley Centre GCMs (HadCM2 and HadCM3) Both GCMs use the same atmospheric horizontal resolution, 3.75° × 2.5° (96 × 72) finite difference model (T42/R30 equivalent) with 19 levels in the atmosphere and 20 levels in the ocean (Johns 1996; Johns et al. 1997). For HadCM2, the ocean horizontal grid lies exactly under that of the atmospheric model. The ocean component of HadCM3 uses much higher resolution (1.25° × 1.25°) with six ocean grid boxes for every atmospheric grid box. In the context of results shown here, the main difference between the two models is that HadCM3 includes improved representations of physical processes in the atmosphere and the ocean (described by Gordon et al. 2000). For example, HadCM3 employs a radiation scheme that explicitly represents the radiative effects of minor greenhouse gases as well as CO_2, water vapour and ozone (Edwards and Slingo 1996), as well as a simple parametrization of background aerosol (Cusack et al. 1998).

The Max Planck Institute fur Meteorologie GCM (ECHAM4/OPYC3) An atmospheric T42 spectral model equivalent to 2.8° longitude × 2.8° latitude (128 × 64) with 19 vertical layers (Roeckner et al. 1996a). The ocean model OPYC3 uses isopycnals as the vertical coordinate system (Oberhuber 1993). As with HadCM3, ECHAM4 also explicitly represents the effects of a range of greenhouse gases and includes an explicit treatment for the radiative effects of aerosols. A full description of the coupled model can be found in Roeckner et al. (1996b).

All the GCMs include sea-ice models and representation of land-surface processes. CSIRO Mk2, GFDL R30 and HadCM2 all include seasonal adjustments of heat and fresh water fluxes at the surface to reduce climate drift in the coupled model simulations. ECHAM4 has annual mean heat and water flux adjustments while HadCM3 has no flux adjustments and maintains a stable control climate simulation.

2.2.2 Model simulations

2.2.2.1 Control From each of the models, we use data from long control simulations that have been performed without any change to the external forcing parameters.

They therefore represent the intrinsic variability of the modelled coupled ocean-atmosphere system. The experiments from which we have data available are a 1000 year control simulation from CSIRO Mk2 (Hirst 1999; Hirst et al. 2000), 990 years of data from HadCM2 (Johns et al. 1997; Tett et al. 1997), 1830 years from HadCM3 (Collins et al. 2001; Johns et al. 2003), 500 years from GFDL-R30 (Delworth et al. 2002) and 240 years from ECHAM4 (Roeckner et al. 1996).

2.2.2.2 Anthropogenic We also make use of a series of simulations of the climate response to anthropogenic forcing. The radiative forcing experiments used here include anthropogenic changes in greenhouse gases and sulfate aerosols. For the CSIRO Mk2, GFDL and HadCM2 models, these changes are expressed as an increase in equivalent CO_2 according to IPCC scenario IS92a along with changes in anthropogenic sulfate aerosols represented through regional changes to surface albedo. For the HadCM3 and ECHAM4 models, increases in individual major anthropogenic greenhouse gases are included, together with explicit treatment of the direct radiative effect of sulfate aerosols. HadCM3 also includes a parametrization for indirect sulfate forcing effects via cloud albedo changes as well as a representation of anthropogenic changes to tropospheric and stratospheric ozone (Johns et al. 2003). From HadCM2 and HadCM3, we have four independent members of an ensemble of simulations with increasing greenhouse gases and sulfate aerosols (GS), three GS ensemble members from GFDL R30, two from ECHAM4 and one from CSIRO Mk2.

2.2.2.3 Natural In addition to the control and anthropogenic forcing simulations, data from transient experiments with changing solar irradiance and volcanic aerosol forcing are also used in the analysis. Variations in the amount of solar radiation reaching the top-of-the-atmosphere form an important external forcing mechanism for climate variability. In the past, changes in the magnitude of solar irradiance have had a significant forcing effect on global climate (Mitchell et al. 2001; Stott et al. 2000a, b, 2001; Tett et al. 1999, 2002). Several reconstructions of past solar variability presently exist, most notably by Lean et al. (1995) and Hoyt and Schatten (1993). Attempts have been made to incorporate both these solar irradiance reconstructions into transient climate change experiments. Here we have available an ensemble of transient simulations from HadCM2 using the solar forcing scenario of Lean et al. (1995), also known as Lean, Beer and Bradley (1995) or LBB (which we shall adopt herein). These simulations have been previously employed in attribution studies by Tett et al. (1999) and Stott et al. (2001). The LBB solar forcing scenario is reconstructed annually from 1610 to 1995 and includes the effect of the 11-year irradiance cycle as well as longer-term variability components. Only the total solar irradiance was altered, not its spectral distribution, nor was any allowance made for possible associated changes in ozone (Stott et al. 2001). Initialisation of the LBB simulations was performed as for the HadCM2 GS runs. Two different periods of estimated solar variations were used in a four-member ensemble for the LBB simulations, one started in the 1751 and finishing in 1860 and three from 1890 to 1997. Since here we are only considering simulated changes corresponding to instrumental observations over the twentieth century, the earlier simulation is discarded so that we effectively use a three-member ensemble of LBB. It is important to note that considerable uncertainty exists in the reconstructed solar irradiance time series, particularly before 1979 (Tett et al. 1999), and that this limitation is implicit in results shown here.

As well as solar irradiance, radiative forcing changes due to volcanic aerosols have also been found to have a significant impact on climate variability, particularly on interannual and decadal time scales (Free and Robock 1999; Shine and Forster 1999; Crowley 2000; Robock 2000). As with solar variability, several reconstructions of volcanic forcing now exist (Sato et al. 1993; Robock and Free 1995; Crowley and Kim 1999; Free and Robock 1999). The reconstructions of Sato et al. (1993) are based on ground-based observations and have been incorporated into a four-member ensemble of transient volcanic forcing simulations using HadCM2. These simulations have been previously employed in the same studies already named (Tett et al. 1999; Stott et al. 2001). The reconstructed volcanic aerosol optical depths of Sato et al. (1993) were applied to the model as monthly values in four 45° zonal bands. Aerosol was spread over model layers between the diagnosed tropopause and 10hPa (Stott et al. 2001). All four of the ensemble members were initialised in the same manner as the HadCM2 GS ensemble. The starting date for volcanic forcing changes is 1850 although only three simulations run till 1995, hence only three are used here. From herein the volcanic forcing experiments shall be referred to as VOL. As with solar irradiance changes, some uncertainty exists in the reconstruction of volcanic aerosol forcing over the twentieth century.

As well as the separate solar (LBB) and volcanic (VOL) forced simulations of HadCM2, we also make use of a four-member ensemble of simulations from HadCM3 forced with the combined solar and volcanic reconstructions as described. These simulations have been analysed by Tett et al. (2002) and Mitchell et al. (2001). The individual ensemble members were initialised in the same manner as the HadCM3 GS runs, with initial conditions taken from different states of the control run, separated by 100 years. This means that both the GS and the combined natural forcing (NAT from herein) ensemble members share the same initial conditions. All four ensemble members are used here for the period 1896–1995. Details of these and other HadCM3 ensembles can be found in Tett et al. (2002).

3 Data coverage

As discussed by Braganza et al. (2003), spatial coverage of the gridded instrumental data is not uniform over time. Large areas of missing data are present in the early part of the record and over Antarctica and the interior of the Southern Hemisphere continents during the entire period. On the global scale however, the suitability of the observational data to estimate climate variability has been established (Jones 1995; Parker et al. 1995). In order to overcome the differences in spatial coverage between the observations and models, Braganza et al. (2003) define a temporally fixed data mask to exclude regions where the observations were sparse or non-existent. This same mask (Fig. 1) is applied here to calculate the indices from instrumental observations and model data.

4 Simple global indices

Five simple global indices of climate change and variability, described by Braganza et al. (2003), are analysed here. They are the global-mean temperature (GM), mean land-ocean temperature contrast (LO), mean magnitude of the annual cycle in temperature over land (AC), the meridional temperature gradient in the Northern Hemisphere mid-latitudes (MTG) and the Northern Hemisphere-Southern Hemisphere temperature contrast (NS). These indices have been based on some of the spatial patterns of climate change that have been used most commonly. While they are not defined to have the same level of uniqueness as spatial fingerprints, the indices do represent the main features of the modelled surface temperature response to increasing greenhouse gases. In addition, defining indices based on large area-averages significantly enhances the signal-to-noise ratio, increasing the probability of climate change detection (Wigley and Barnett 1990; Stott and Tett 1998). Braganza et al. (2003) also show that interannual and decadal variations in four of the indices (GM, LO, AC, MTG) are reasonably independent for unforced climate whilst showing a coherent response for greenhouse climate change. Considered collectively, these indices therefore provide information in addition to the global mean alone and provide a useful signal of greenhouse climate change.

The surface temperature data used to calculate the indices are anomalies relative to a 30-year reference period from the control simulations for model data and relative to the period 1961–1990 in the observations (Jones et al. 1999). Annual means were constructed as in Braganza et al. (2003) using seasonal averages from December of the previous year to November. Time series of the indices from all data sources have been rescaled relative to 1881–1910. In order to estimate variability on decadal time scales, the interannual time series are filtered with a low-pass, 21-point binomial filter (half power at periods near 10 years) as used in Braganza et al. (2003) and IPCC TAR (Folland et al. 2001). A full definition of the indices, including their association with aspects of the large-scale atmospheric circulation, is given by Braganza et al. (2003).

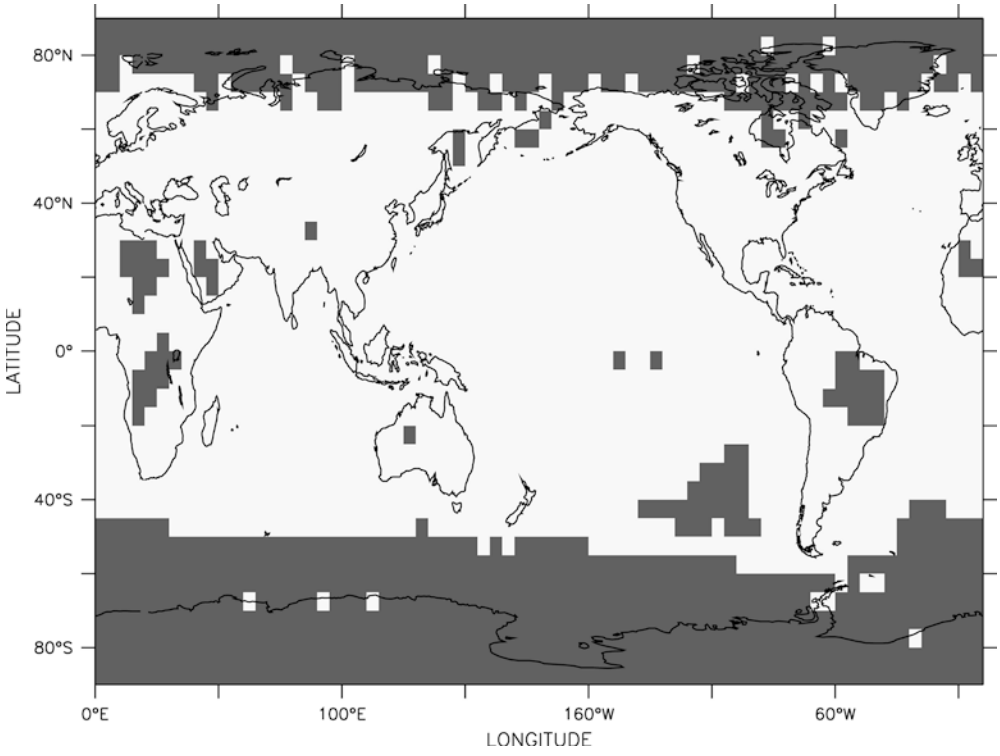

Fig. 1 Data mask used in the calculation of the indices from both observed and modelled data. *White areas* indicate regions included in the analysis. *Shaded areas* indicate regions of sparse coverage (less than 40 years of data since 1900) that were excluded from the analysis

*Global-mean surface temperature (***GM***):* studies of climate change detection commonly use some measure of global-mean surface temperature. Here we simply take the area-weighted global average of surface temperature.

*The contrast between land and ocean surface temperature (***LO***):* LO is defined as the difference between mean surface air temperature (SAT) over land and mean sea surface temperature (SST). This index has been chosen to capture the pattern of greater and more rapid warming over land than ocean (SAT - SST) that has been identified in previous studies (Jain et al. 1999; Meehl et al. 1993).

*The inter-hemispheric difference in surface temperature (***NS***):* NS is defined as mean Northern Hemisphere (NH) temperature minus the mean Southern Hemisphere (SH) temperature. This index has been chosen to represent the influence of anthropogenic sulfate aerosols in the NH, which contribute to relative cooling in the NH (Kaufmann and Stern 1997; Meehl et al. 1993; Santer et al. 1996; Wigley et al. 1998).

*The mean magnitude of the annual cycle in temperature over land (***AC***):* The magnitude of the annual cycle was calculated for each hemisphere by subtracting mean winter from mean summer surface temperature over land. These quantities were then area-weighted by the fraction of global land surface area in the respective hemisphere and combined into a single index.

$$\mathrm{AC} = \mathrm{W_{NH}}\langle \mathrm{JJA} - \mathrm{DJF} \rangle + \mathrm{W_{SH}}\langle \mathrm{DJF} - \mathrm{JJA} \rangle$$

Note that AC is effectively the seasonal range between winter and summer temperatures and will be somewhat less than the magnitude of the annual cycle estimated by fitting a sinusoid to the monthly temperatures. The variations of AC computed here are highly correlated with those calculated from fitting a sinusoid to monthly data. AC has been chosen to represent the range of the annual cycle of temperature, which has been shown to be decreasing overall in the observations mainly as a result of increased warming over land during winter (Thomson 1995; Mann and Park 1996).

*The mean meridional temperature gradient in the NH mid-latitudes (***MTG***):* MTG is defined by taking the difference in area averaged surface temperature from mid to high latitude and sub-tropical zonal bands in the NH hemisphere.

$$\mathrm{MTG} = \langle 52.5^{\circ}\mathrm{N} - 67.5^{\circ}\mathrm{N} \rangle - \langle 22.5^{\circ}\mathrm{N} - 37.5^{\circ}\mathrm{N} \rangle$$

This index has been chosen to represent the expected high latitude amplification of the warming due to increasing greenhouse gases (Manabe and Stouffer 1980; Wigley and Barnett 1990) and the recent observed pattern of greater warming in high latitudes compared to the tropics (Gitelman et al. 1997, 1999; Jain et al. 1999). A positive trend in MTG corresponds to a reduction in the equator-to-pole temperature gradient.

5 Observed and simulated trends in the indices during the twentieth century

We first compare observed trends in the indices with those in forced model simulations. Time series of decadal scale variations in each of the observed indices are plotted against the ensemble mean trends from GS simulations from all of the models (Fig. 2). Error bars indicate the uncertainty at the 5–95% confidence level associated with ensemble sampling for an individual realisation. For the latter part of the twentieth century, large changes are found for GM, LO and AC in the context of the previous 100 years. Large changes are also found in MTG, although the signal is less clear due to larger interdecadal variability. GS forced simulations from all models produce similar trends to those observed in surface warming (GM), increased warming over land (LO) and increased warming at higher latitudes (MTG) but underestimate both the decadal variability and the negative trend in the magnitude of the annual cycle (AC). This is attributable to less warming and decadal variability in surface temperature over land during winter in the forced simulations compared to observed changes during the last 50 years.

Figure 3 shows the magnitude of 50 and 100-year linear trends in observations and GS experiments over three time periods from the low-pass filtered time series. Fifty-year trends from the first half (1900–1949) and last half (1950–1999) of the century are shown along with the 100-year trend from 1900–1999. For the GS experiments, uncertainties in the magnitude of the mean trends are the 5%–95% confidence interval for the distribution of 50 and 100-year linear trends (sampled at 10 year intervals) from the long control simulations. Linear regression analysis presented in the following section shows that estimating the uncertainty in the forced trends from the control is reasonable since the magnitude of the ensemble sampling error can be attributed to the intrinsic variability in each of the models. No uncertainty estimates are shown for ECHAM4 since the length of the control integration used here is relatively short. Inspection of the mean 50 and 100-year trends in the indices from control climate simulations shows that the distribution of trends for each index is similar in all the models. For all the indices, unforced 50 and 100-year linear trends are normally distributed about zero. By contrast, the magnitude of observed changes over the last 50 years are significantly different to the range of trends expected due to modelled internal variability for all indices except NS (hemispheric temperature contrast). Since the models simulate reasonably realistic internal

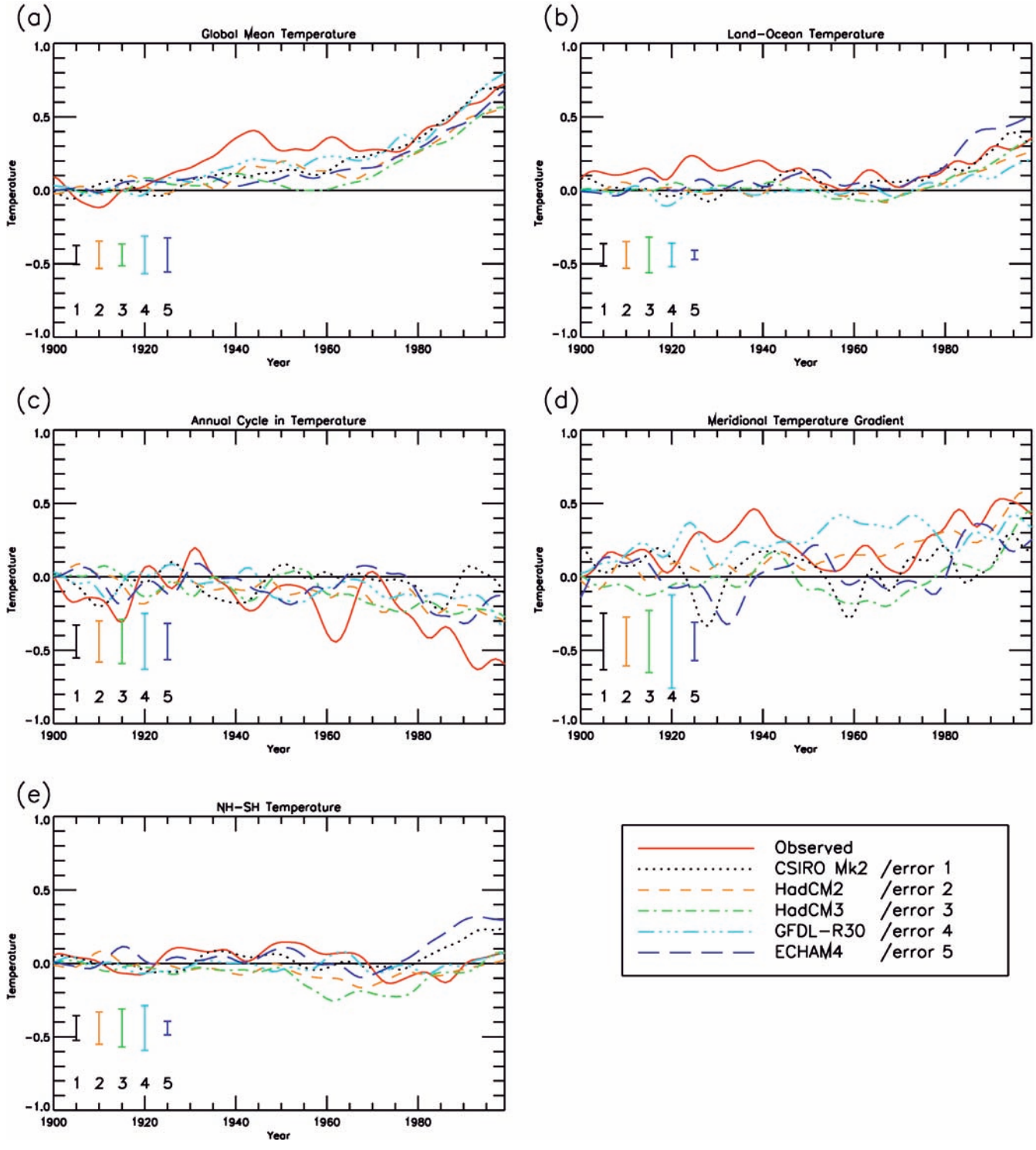

Fig. 2a–e Decadal smoothed ensemble mean timeseries of indices from observations and model GS runs for the period 1900–1999. Error bars represent the 5–95% confidence interval associated with ensemble sampling uncertainty, except for CSIRO Mk2, where uncertainty is estimated from the decadal scale variability in the control

variability in the indices (Braganza et al. 2003), here we will use uncertainty estimated from HadCM3 to represent uncertainty in the observations. HadCM3 has the largest variability across all of the indices and the longest control simulation. Uncertainty in the observed linear trends is indicated in Fig. 3 as an error bar about zero for each index. A linear trend is defined as significant when uncertainty in the simulated trend does not overlap with the 5–95% confidence interval for the distribution of trends from internal variability.

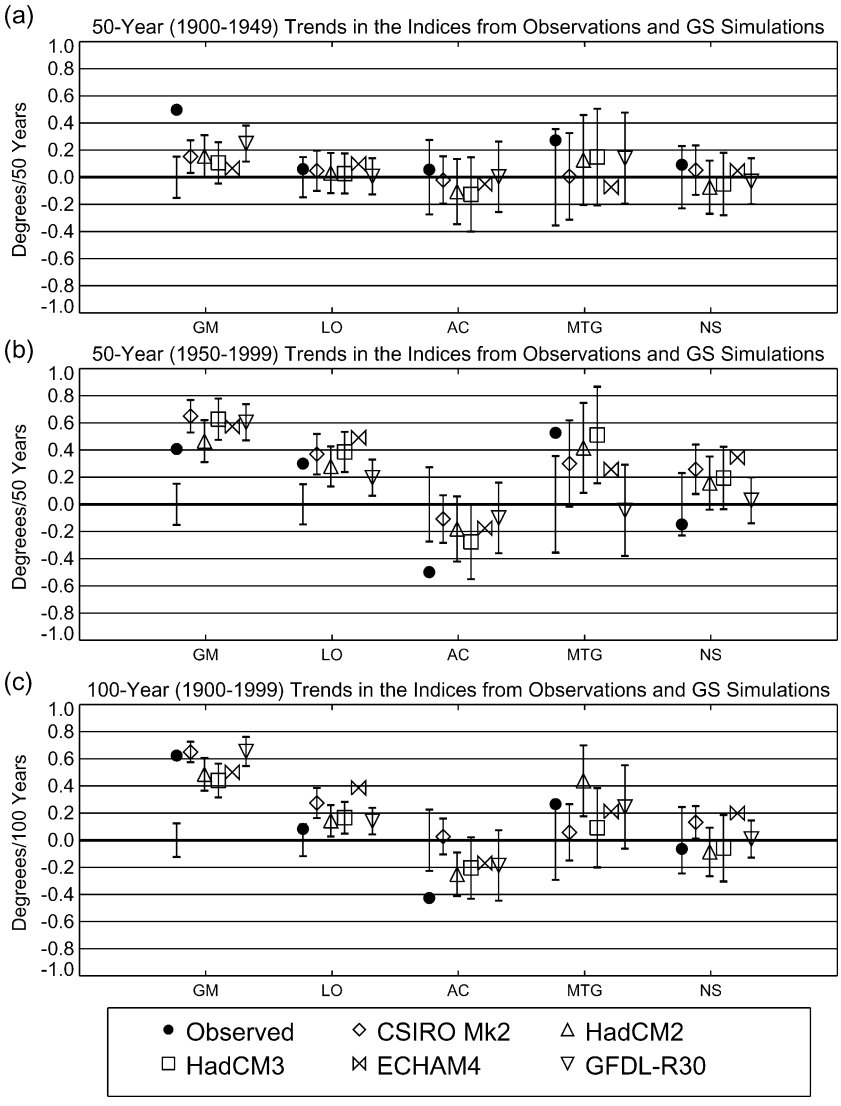

Fig. 3a–c Estimated linear trends in the indices from observation and GS simulations over three periods, 1900–1949, 1950–1999, 1900–1999. Error bars represent the 5–95% confidence interval estimated from the distribution of trends in the control for each model except ECHAM4 for which there is only 240 years of control data. Uncertainty due to intrinsic climate variability is estimated from the 5–95% confidence interval from HadCM3 control integration and represented as an error bar about zero for the observations

While the mean observed 100-year trends for 1900–1999 are significant in GM (0.62 °C) and AC (–0.43 °C) and relatively large for MTG (0.27 °C), the temporal response in the indices is markedly different between the first and second half of the century. During the first 50 years, observed and modelled trends in each of the indices were not significantly different to estimates of natural variability, except for GM which warmed by 0.5 °C in the observations. For LO, AC and MTG, the signal of climate change is largest over the last 50 years. For this period, there is statistical consistency (considering estimated uncertainty due to intrinsic climate variability and estimated ensemble sampling error) between GS simulations and observations in the majority of models and for all of the indices except NS. Changes in the annual cycle are too small in the models over the last 50 years while GFDL-R30 shows no trend in MTG over the same period. For NS, recent observed trends are small and of opposite sign to those in the GS forced experiments. In general however, the consistency between the observed trends and the magnitude of the GS response in LO, AC and MTG indices, as well as GM, provides additional evidence for anthropogenic influence on climate over the last 50 years. It should also be noted that none of the GS simulations, except perhaps GFDL R30, can explain the observed GM increase during the first half of the twentieth century.

Figure 4 shows 50, 45 and 100-year trends for three different periods, 1900–1949, 1950–1994 and 1895–1994 for GS, LBB and VOL simulations from HadCM2 and for GS and NAT simulations from HadCM3. These periods do not correspond exactly to the GS analysis described already, where trends were compared for the period 1900–1999, since the naturally forced simulations are available until 1994 only. As with GS forced simulations, estimated 50-year trends in the indices due to natural forcing are not significantly different to zero during the early century. For changes in the latter half of the century, HadCM3 NAT and HadCM2 LBB also produce no significant trends in the indices. Volcanic aerosol forced trends in global mean temperature in HadCM2 are significant for the same period, although of the opposite

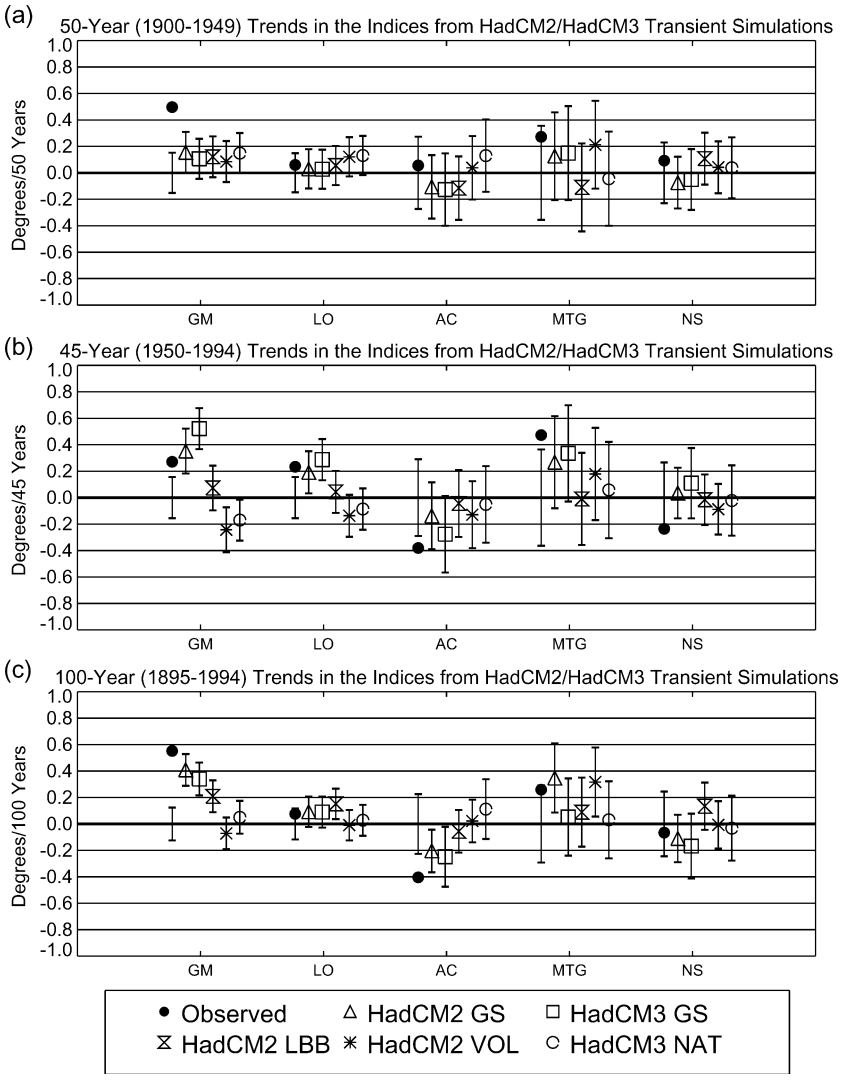

Fig. 4a–c Estimated linear trends in the indices from observation and GS and naturally forced simulations from HadCM2 and HadCM3 over three periods, 1900–1949, 1950–1999, 1900–1999. Error bars represent the 5–95% confidence interval estimated from the distribution of trends in the control. Uncertainty due to intrinsic climate variability is estimated from the 5–95% confidence interval from HadCM3 control integration and represented as an error bar about zero for the observations

sign to the observations, and similar to HadCM2 GS for MTG. For century scale linear trends, only the GS runs produce changes in GM similar in magnitude to the observed. The steady increase in solar forced GM in HadCM2 over the whole of the twentieth century is reflected in the magnitude of the 100-year trend, which is significantly larger than zero (0.2 °C), but not consistent with the magnitude of the observed warming. Volcanic forcing in HadCM2 produces a significant trend in MTG that is comparable with both observations and GS forcing. The suggestion in these results is that, while changes due to natural forcing are not generally larger in magnitude than those expected due to intrinsic climate variability, they may have in part contributed to observed changes in global mean temperature and meridional temperature gradient over the whole of the twentieth century.

6 Time dependent changes in the indices

While comparison of the magnitude of trends provides some information about the mean response or sensitivity to GS and natural forcing, it is perhaps not the best method of investigating time dependent changes in the forced response. Since the assessment of human influence on climate would be greatly aided by the attribution of recent observed changes to one *or more* forcing mechanisms, as well as an assessment of the influence of intrinsic variability or noise, we need some method of assessing the relative contributions that multiple forcing factors make to observed climate change. In this section, we compare the mean temporal evolution of the indices between observations and forced simulations and determine whether the residual decadal time scale variability is consistent with estimates of internal variability or attributable to some other, additional forcing mechanism.

As outlined earlier, a common approach to attribution (following from Hasselmann 1993) is to test for consistency in the signal amplitude of observations and GCM transient forced simulations. This approach is based on the assumption that observed changes S may be represented as a linear sum of the response to l different forcing signals and internal climate variability or noise $\mathbf{N}$.

$$S = \sum_{i=1}^{l} \beta_i F_i + \mathbf{N} \quad (1)$$

with β_i representing the amplitude or amount by which we have to scale the ith response signal F in order to match observations. Equation 1 can be rewritten to explicitly include the anthropogenic and natural simulations used here;

$$S = \beta_1 \mathbf{GS} + \beta_2 \mathbf{LBB} + \beta_3 \mathbf{VOL} + \mathbf{N} \quad (2)$$

or

$$S = \beta_1 \mathbf{GS} + \beta_2 \mathbf{NAT} + \mathbf{N} \quad (3)$$

While many different variations of this approach have been taken it has been shown (Allen and Tett 1999) that such methods are basically variations of linear or multiple-linear regression techniques. It has also been shown (Allen et al. 2000; Tett et al. 2002) that regression analysis reduces the impact of uncertainties in the climate response to forcing, such as the climate sensitivity, by providing estimates of the relative linear contributions of external forcing mechanisms and internal variability to the climate change signal. Several recent studies (Stott et al. 2000a,b, 2001; Tett et al. 1999, 2002; Hegerl et al. 1997) have used multiple linear regression techniques to assess the relative influence of multiple radiative forcings in observed changes. Chapter 12 of the IPCC TAR (Mitchell et al. 2001) contains estimates of scaling factors for the amplitude of anthropogenic and naturally forced model simulated signals for a range of GCMs. Whereas the majority of previous studies have applied these techniques to estimate the amplitudes of space-time varying signals in an optimal fingerprint framework, our test statistic is simply the climate change indices, considered individually and collectively as a normalised single index. This approach simplifies the analysis of results while still providing additional information for attribution through the spatial information contained in the indices themselves. Previous fingerprint pattern correlation studies (Santer et al. 1993) have noted that failure to detect greenhouse signal patterns in observations may be due to the signal being obscured by noise associated with internal climate variability. In this regard, determination of the signal-to-noise ratio of the global indices is somewhat simpler and easier to interpret than spatially normalised optimal fingerprints.

We use a simple form of linear regression (*ordinary least squares*) to investigate the amplitude consistency between observed and simulated changes in the indices. In an attribution context, linear regression analysis allows us to describe a relationship between the means of the observed signal (dependent data) and the simulated forced response (independent data) so that we may formulate a linear relationship as in Eq. 1 that provides a realised value of S predicted by the sum of the forcings. Here we apply single linear regression to describe the relationship between observations and the GS forced response as well as multiple linear regression to investigate the relationship between observations and the combined response due to anthropogenic and natural forcing. For multiple regression, the independent data are treated as a matrix of independent time series (simulated forced responses) whose linear combination is fitted to the observed timeseries. The resultant timeseries is referred to as the *realised response* (best fit) from the linear combination of forced signals. The resultant scalar linear regression coefficients (β_i in Eq. 1) represent the scaling required for the amplitude of the forced response in order to be consistent with observed changes.

In an attribution context, estimating uncertainty in the amplitude scaling of model simulated signals is useful in determining the amplitude consistency between observed changes and the simulated forced response. In order to determine a confidence region for the amplitude scaling for the indices, we must estimate the variance of the linear regression coefficient. Since the regression coefficient is a linear function of the observations, which we assume to be normally distributed, we may then assume that β_i is also normal. The variance of β_i may then be estimated from the variance in the residuals (regression model error) divided by the sum of squared departures from the mean of the independent data (Myers 1986). Here this is represented as

$$\sigma_\beta^2 = \sigma_N^2 / sse_F \quad (4)$$

where ${\sigma^2}_N$ is the variance of the intrinsic noise term $\mathbf{N}$ in the regression Eq. 1 and sse_F is the sum of squared departures from the mean of the simulated forced time series. Previous studies, (Allen et al. 2000; Stott et al. 2001; Tett et al. 2002) have derived uncertainty estimates in observed and model responses from numerical simulations. Following from these studies the intrinsic climate noise is perhaps best estimated from the control integration. While it has also been noted that deriving uncertainty limits from simulations may be considered a significant source of uncertainty in itself (Tett et al. 2002), Braganza et al. (2003) show that this is a reasonable approach in the context of the climate change indices used here. We define a measure of noise which we call the *noise variance* (${\sigma^2}_N$), calculated as the sum of the mean 100-year internal variance from the control (${\sigma^2}_i$) and the ensemble variance (${\sigma^2}_e$) divided by the number of ensemble members N_e,

$$\sigma_N^2 = \sigma_i^2 + \sigma_e^2 / N_e \quad (5)$$

The mean internal variance ${\sigma^2}_i$ is calculated from 100 year samples taken at 50 year intervals from the low-pass filtered control run as in Braganza et al. (2003). Since the regression results were found to be sensitive to decadal variability, the low-pass filtered data was further smoothed by taking the decadal mean, spaced evenly at 10-year intervals, so that the variability and regression analysis are both performed using 10 decadal-mean values over the 100 year time series or samples. The relative shortness of this record forms a limitation in this work.

The noise variance allows us to take into account the internal noise estimate for the observations (from the control) and the uncertainty in the forced response (from the ensemble mean or sampling noise) when calculating uncertainty in the amplitude scaling. For each model, $\sigma^2{}_i$ and $\sigma^2{}_e$ are found to be very similar indicating that variability between ensemble members is associated with the intrinsic climate variability of the model. Here we use the HadCM3 control run to calculate $\sigma^2{}_i$ since it gives the largest estimates of internal variance across all the indices. Confidence intervals for the noise variance are calculated using the resampled variance (var) of $\sigma^2{}_i$ from HadCM3 control as in Braganza et al. (2003). The variance of $\sigma^2{}_N$ is therefore estimated as

$$\mathrm{var}(\sigma_N^2) = \mathrm{var}(\sigma_i^2)(1 + 1/N_e) \ . \quad (6)$$

Amplitude consistency tests were performed using single linear regression analysis over the period 1896–1995 for the observed and GS response from each of the five models and using multiple linear regression analysis over the same period for the GS and naturally forced responses from HadCM2 and HadCM3. Figure 5a shows the amplitude scaling factor (linear regression coefficient β_1) for the GS response in each of the models and for each of the indices as well as the associated 5–95% confidence interval. As well as the five indices, also shown is the scaling for the single or combined normalized index (CNI), composed of the indices GM, LO, AC and MTG. In order to apply linear regression across all of the variables, the timeseries must have zero mean and uniform variance. Hence, the CNI was constructed by concatenating the zero-mean, normalized time series of each of the indices into a single 400-year (40 point) decadal time series. The control 100-year mean standard deviation was used to normalise the data. As a check of the internal variance estimate, σ_N was calculated for the normalised index and was found to be very close to $\sqrt{(1 + 1/\mathrm{N}_e)}$for each model. The NS index has been omitted from the CNI since it has been shown here to

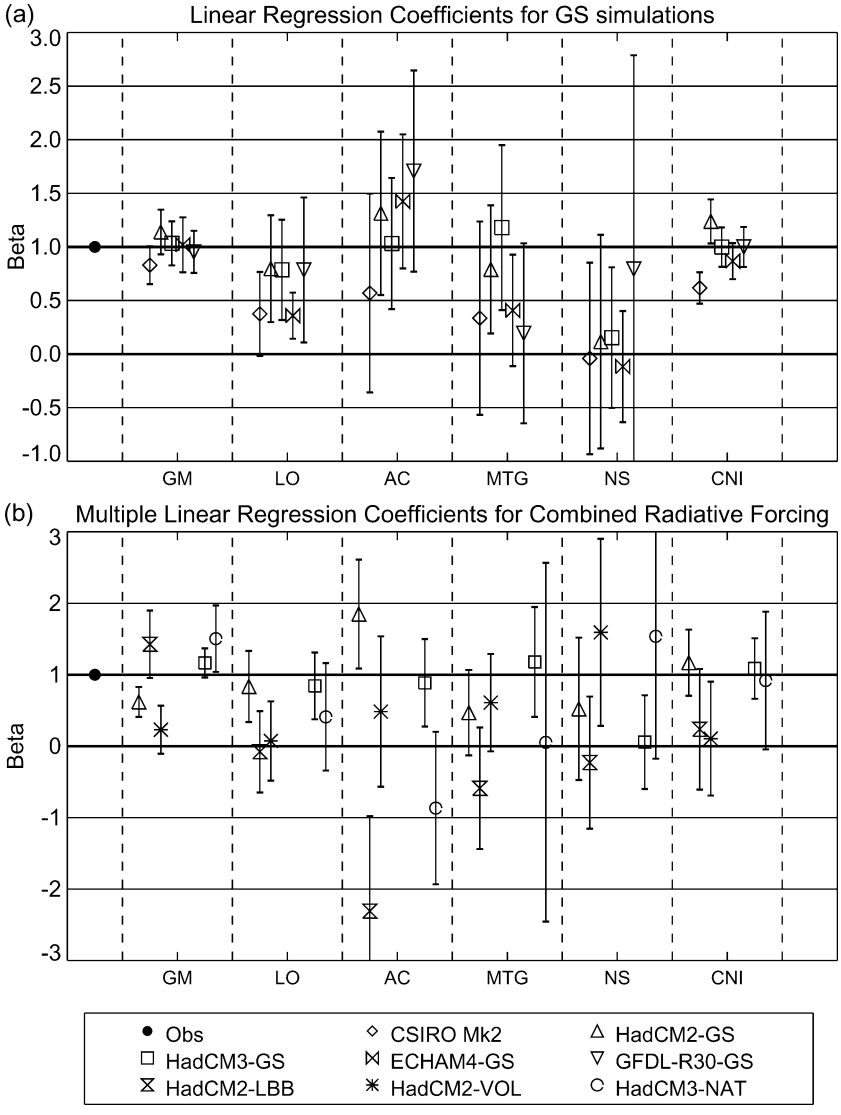

Fig. 5 **a** Single linear regression coefficients (β) representing the scaling amplitude of the GS model response for each index compared to the observed (unity). **b** Multiple (linearly combined) regression coefficients representing GS, SOL, LBB and NAT amplitude scaling. Error bars represent uncertainty in scaling at the 5–95% confidence interval

display no significant response to anthropogenic forcing. In addition, Karoly and Braganza (2001) and Braganza et al. (2003) showed that NS is highly correlated with LO for internal variations.

Following Tett et al. (2002) we test that the amplitude of the simulated forced response is consistent with that of the observed signal. If the two-tailed uncertainty includes unity then we infer consistency in the signal amplitude at the 90% confidence level. Similarly, if the uncertainty includes zero, then we conclude that there is no significant signal of forcing present in the observations. Amplitude consistency plots for GS forcing are shown in figure 5a. A significant anthropogenic climate signal can be detected separately in the observed LO and AC indices in all models except CSIRO, as well as in GM. For NS, the amplitude scaling for all the models is not significantly different to zero, indicating that an anthropogenic climate signal cannot be detected in the interhemispheric temperature contrast. For GM there exists remarkable amplitude consistency in all but the single GS realisation of CSIRO Mk2 which falls just outside the confidence region. Similarly for LO of CSIRO Mk2 and ECHAM4 where the response is too small, as evidenced by the magnitude of the linear trends. For CNI, consistency is found in HadCM2, HadCM3 and GFDL-R30 but not in ECHAM4 (2 member ensemble) and CSIRO Mk2 (single run) at the 90% confidence interval.

Along with the amplitude consistency, further information may be extracted from the linear regression analysis by making use of the noise estimates we define in the preceding section. As in Braganza et al. (2003), where the variance of the detrended residuals from the observations and transient experiments were compared to the unforced variability of control simulations, the error between the realised response and the actual observed timeseries may be compared to the noise variance σ^2_N defined above. Differences between the realised response and observations may be expected to contain more information than residuals calculated by removing a polynomial trend (as in Braganza et al. 2003) since the realised response effectively represents the estimated contribution of the forced response to the observed signal. If these residual errors are consistent with the noise variance estimate then we may infer that the observed signal is composed of the scaled forced response plus intrinsic climate noise as in Eq. 1. As discussed previously, given that the variability of the indices in the control integrations of all the models is realistic, a large mean residual error compared to internal noise suggests that the observed signal contains responses to unidentified forcings or processes (e.g. land-surface changes), or errors in the simulated variance and observations.

Figure 6 shows the mean sum of squared errors (MSE) taken from the difference between the observed trend and fitted response for GS forcing alone, plotted against internal variance for GM and CNI. Both values shown are degrees Celsius scaled by a factor of $\times 100$. If the two-tailed uncertainty in the estimated internal variance encompasses the MSE than we infer some consistency between climate noise and residual errors. For changes to global mean surface temperature (GM), only the GFDL-R30 simulation has residual errors that are consistent with unforced climate variability. For HadCM3 GM, the magnitude of residual variability is large when compared to intrinsic climate noise and suggests either errors in the simulated forced response or that other forcing factors may contribute to the observed signal. This result highlights the problems in attributing climate change using global mean alone. For the combined index (CNI), no significant differences are found between the internal variance and MSE in any of the models.

This leads us to consideration of the relative contributions of GS *and* naturally forced responses to the observed signal. Figure 5b shows the multiple regression coefficients or linearly combined amplitude scaling for each index and forcing, as well as the combined normalized index, along with uncertainties at the 5–95% confidence interval. Looking first at HadCM2, the anthropogenic forced response makes a statistically significant contribution to GM, LO and AC but not to

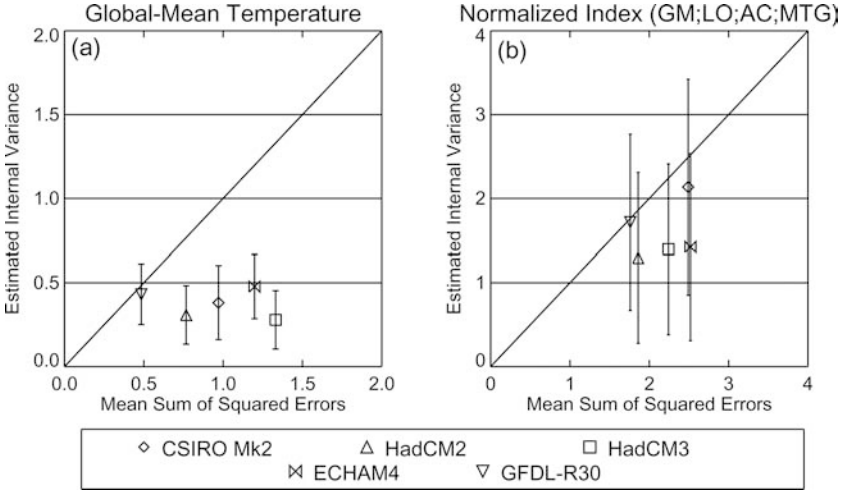

Fig. 6 Mean sum of squared errors (MSE) from the linear response (best fit) in **a** GM and **b** CNI versus the noise variance (σ^2_N). Error bars represent the 5–95% confidence interval for σ^2_N. Values are degrees Celsius $\times$ 100

MTG and NS. GS amplitude scaling is consistent with observations only for LO, with the relative contributions from the solar and volcanic aerosol LO responses consistent with zero. For the realised GM response, the amplitude of the GS response is too large compared to the observed (i.e. the required amplitude scaling is less than 1). The LBB forced global-mean temperature was found to be both highly correlated with (0.91) and consistent in amplitude with observations. While the magnitude of the LBB GM response is much smaller than the response to GS forcing, amplitude consistency is inferred due to larger uncertainties in the scaling of the LBB signal. For AC, both LBB and VOL forcing make possible zero contributions while the GS contribution needs to be scaled upward as may be expected from inspection of the linear trends. Interestingly, both anthropogenic and volcanic forced MTG responses in HadCM2 are equally scaled and are both highly correlated (0.65 and 0.70 respectively) with the observed changes. However considering uncertainties, both forcings make potential zero contribution to the realised response. The observed changes in NS show reasonable correlation with VOL forced changes (0.60) as well as amplitude consistency. For the combined normalised index (CNI), anthropogenic forcing is consistent with the observed while solar and volcanic aerosol forced signals make possible zero contributions to the multi-forced realised response with large uncertainties.

For HadCM3, a more uniform result is seen across the indices with consistency in the amplitude of the GS signal for GM, LO, AC and MTG individually, indicating that the GS signal is detectable separately in each of these indices even when a naturally forced signal is also considered. However, NAT forcing is found to have a significant influence on GM (but not the other indices) after uncertainties are included. We may infer from comparison with LBB and VOL GM signals that this result is dominated by the solar forcing response. For the combined index (CNI), only the GS forced response makes a significant contribution to the observed index. While the amplitude scaling of the NAT forced CNI signal is of equal magnitude to observations, consistency can not be inferred due to large uncertainty.

It must be noted that for weak forced signals, a potential source of uncertainty comes from the sensitivity of the scaling amplitudes to the use of ordinary least squares regression. Recent work (Allen and Stott 2002) has shown that ordinary least squares regression underestimates the amplitude scaling for weak signals and small ensembles. There is therefore the potential that the amplitude of naturally forced signals is underestimated here. Sensitivity to ordinary least squares is not likely to affect the amplitude estimate for GS forcing, as this is a stronger signal in the second half of the century.

Amplitude scaling factors for CNI may be compared with optimal fingerprint scaling factors from HadCM2, HadCM3 and ECHAM3/LSG from Mitchell et al. (2001), who consider the simultaneous contribution of individual forcing signals from greenhouse gas, sulfate aerosol, solar, volcanic aerosol and combined solar and volcanic aerosol simulations (see Fig. 12.12 from Mitchell et al. 2001). Since greenhouse gas and sulfate aerosol forcing are considered separately, we compare GS forcing used here with greenhouse gas only forcing from Mitchell et al. (2001) and find that scaling amplitudes for CNI are consistent with those for optimal fingerprints for HadCM2 and HadCM3. Similarly, scaling of the VOL CNI response is also consistent with that for volcanic aerosol optimal fingerprints in these two models. While estimations of NAT and LBB scaling differ, the relative contribution of the natural forcing responses (ie possibly zero with large uncertainties) is consistent.

7 Contribution to global warming

Estimates of the contribution to observed changes from anthropogenic and natural forcing factors may be derived by combining the estimates of amplitude scaling from the models with the magnitude of the simulated forced response. As shown by Mitchell et al. (2001), optimal fingerprint scaling factors may be applied to the global-mean temperature to estimate the contribution from forcing changes to observed global mean warming over the twentieth century (see Fig. 12.12, Mitchell et al. 2001). In a similar manner, here we apply the CNI amplitude scaling to the model predicted change in GM. We calculate estimated contributions from each of the forcing simulations considered here to global warming over three periods, the whole of the twentieth century (1896–1995), the latter part of the twentieth century (1946–1995) and the early part of the twentieth century (1896–1945). Figure 7 summarises these estimates for GS forcing in all the models, and for the linear combination of GS and natural forcing in HadCM2 and HadCM3. Results for the period 1946–1995 are not shown since they are similar to those for the whole century. In order to calculate uncertainties in the contribution to global warming from radiative forcing changes we take into account uncertainty in the scaling amplitude and uncertainty in the simulated forced response. Uncertainty is estimated by taking the product of the variance for two independent, normally distributed variables. In this case our variables are the CNI amplitude scaling X,

$$X \sim N(\beta, \sigma_\beta^2)$$

and the forced change in GM from the model simulations Y,

$$Y \sim N(T, \sigma_T^2) \ .$$

We can estimate the variance in the contribution to global warming XY as,

$$\mathrm{var}(XY) = \sigma_\beta^2 \sigma_\gamma^2 + \sigma_\beta^2 T^2 + \sigma_T^2 \beta_i^2 \ . \qquad (7)$$

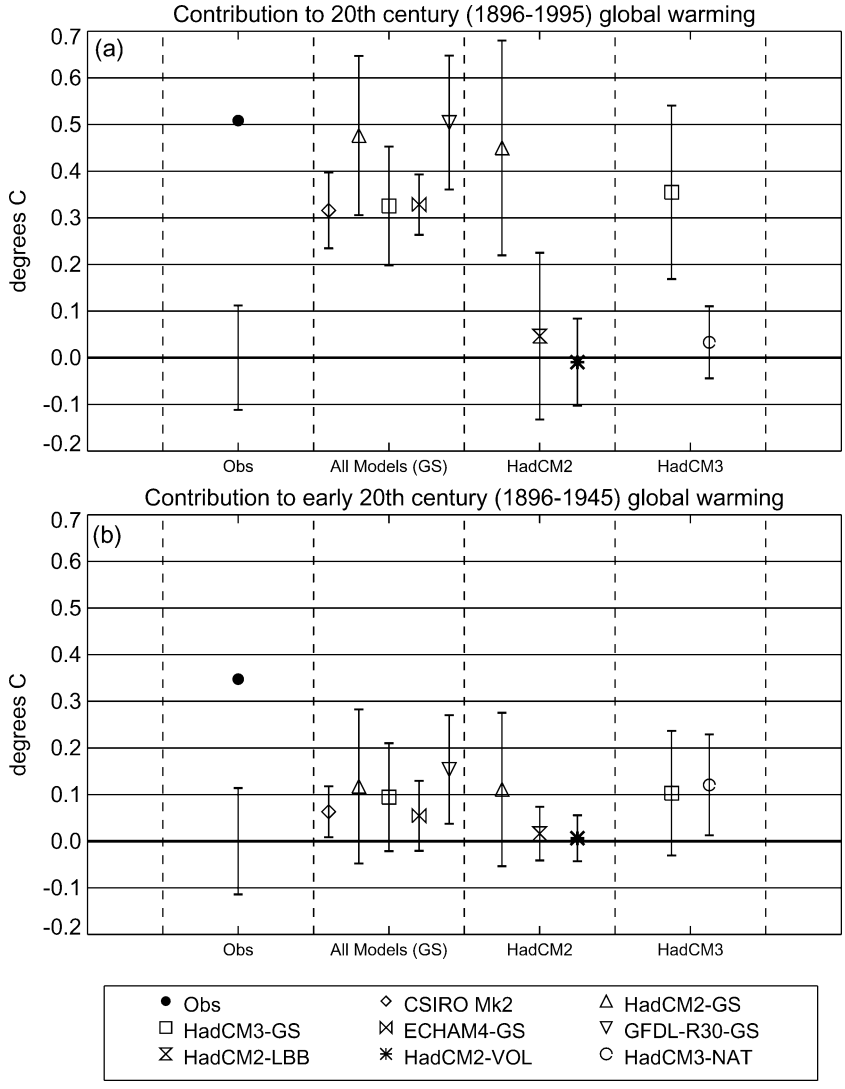

Fig. 7 **a** Estimated contribution to global warming over the twentieth century (1896–1995) **b** Estimated contribution to global warming during the early twentieth century (1896–1945). Calculated as changes in GM from anthropogenic forcing (all models GS) and relative changes in GM from combined anthropogenic and natural forcing (HadCM2 and HadCM3) from the multi-decadal smoothed time series and scaled with CNI amplitude scaling. Error bars represent the 5–95% confidence interval estimated from uncertainty in CNI amplitude scaling applied to the estimated changes in GM. The observed change is calculated from the multi-decadal smoothed time series with the uncertainty taken from the 5–95% confidence interval from the distribution of trends from HadCM3 control integration

The mean change T in GM is calculated as the ensemble mean linear trend from the multi-decadal smoothed time series. The variance of T is estimated from the range of trends found in the control integration.

Figure 7 shows estimated contributions to global warming from anthropogenic and natural forcing with uncertainties at the 5–95% confidence interval. Uncertainties in the magnitude of observed changes are estimated using the range of multi-decadal trends from the HadCM3 long control integration. Considering the period 1896–1995, GS forcing alone (Fig. 7a, panel 2) produces scaled changes in GM that are consistent with observed changes and internal variability. For multiple forcing (Fig. 7a, panels 3 and 4), GS forcing contributes most to the observed warming with smaller and statistically insignificant contributions from natural forcing. These results are consistent with those shown in Fig. 12.10b from IPCC TAR.

Figure 7b shows the estimated contribution to global warming during the early twentieth century. GS forcing alone (Fig. 7b, panel 2) makes a non-zero contribution to global warming in only two models, CSIRO Mk2 (0.06 °C) and GFDL-R30 (0.15 °C). Such changes cannot fully account for the magnitude of observed change (0.35 ± 0.11 °C) to global mean temperature for 1896–1945. Previous studies (Stott et al. 2001; Tett et al. 2002) have suggested that large changes to observed global mean surface temperature during this period are more likely to be explained by a combination of forcing factors rather than dominated by greenhouse gas changes. This is supported here in analysis using HadCM3 (Fig. 7b, panel 2), which shows that anthropogenic forced changes (0.10 ± 0.13 °C) and naturally forced changes (0.12 ± 0.11 °C), as well as maximal changes due to intrinsic variability (± 0.11 °C) may explain observed global mean surface warming for the early twentieth century.

Since all of the forced signals are weak and the uncertainties larger during the early part of the twentieth century, a number of considerations need to be taken into account when assessing the relative contributions to the observed response. It has been noted previously

(Johns et al. 2001; Stott et al. 2001; Allen and Stott 2002) that the ability to detect naturally forced signals is sensitive to the various choices made in the methodologies. While the scaled warming in HadCM2 shows possible zero contributions from natural forcing, estimated changes for this period were found to be highly sensitive to the sampling period of the multi-decadal time series, particularly for the VOL forced response. By changing the sampling period, it is possible to detect a non-zero contribution to global warming due to changes in volcanic aerosol forcing. The sensitivity of VOL detection to sampling is consistent with that of Stott et al. (2001) for decadal averages on 50 year time scales. The estimate of natural contributions to the observed warming may also be sensitive to the use of ordinary least squares regression.

8 Summary

Over the last 50 years, observed linear trends in the global-mean temperature (GM), the land-ocean temperature contrast (LO), the magnitude of the annual cycle in temperature over land (AC) and the Northern Hemisphere meridional temperature gradient (MTG) are found to be significantly larger than changes expected due to internal variability and changes in solar and volcanic aerosol forcing. Good agreement is found between the observed trends and greenhouse gas plus sulfate aerosol (GS) forced response in all of the indices except the hemispheric temperature contrast (NS), which displays no climate change signal, and the magnitude of AC, which shows a large negative trend in the observations that is consistently too small in each of the models analysed here. Consistency between the observed and GS trends in four different indices suggests that anthropogenic forcing has had a large influence on observed changes during the later part of the twentieth century.

Single and multiple linear regression of the observed and modelled response of the indices to different radiative forcing factors provides useful information for the attribution of recent observed climate change. Signal amplitude consistency tests were performed to compare anthropogenic forced changes to observed changes in each of the five climate models considered here. The magnitude of GS simulated and observed responses of each of the surface temperature indices as well as a combined normalised index (CNI) were tested for consistency. In addition, amplitude scaling was calculated for simultaneous (linearly combined) anthropogenic and naturally forced responses from HadCM2 and HadCM3. Results from this analysis reveal the relative importance of anthropogenic, solar and volcanic aerosol forcing, as well as intrinsic climate noise, in the observed changes in the indices. For the four climate change indices, GM, LO, AC and MTG, there is good agreement in the amplitude of the observed and GS signals in almost all of the models. In addition, the GS-forced model simulations show reasonably high correlation with observed changes, although results vary between the models. For global mean temperature, results indicate that GS forcing has a significant influence on changes during the twentieth century and dominates the climate change signal over the last 50 years. For the early part of the century, changes to GM may be explained by a combination of natural and GS forcing, as well as internal climate variability. This result is consistent with the IPCC Third Assessment Report (Mitchell et al. 2001) and several recent studies (Stott et al. 2000a, 2000b, 2001; Tett et al. 1999, 2002). The GS forced response is also found to dominate the observed LO signal.

For changes to AC, we may infer from multiple regression analysis that differences between the large observed trend and the more modest GS forced response are unlikely to be explained by contributions from solar or volcanic forcing. Similarly, comparison of residual errors between the observed and realised response due to multiple forcing with estimates of unforced climate variability suggest that these differences are also unlikely to be explained by uncertainty due to climate noise. It is therefore likely that the GCM simulation of AC is inadequate or that the observations are responding to some as yet unknown forcing. Of all the models considered here, changes to AC are largest in HadCM3. This model includes more realistic representation of clouds, including some representation of the indirect effect of increasing aerosols on clouds, and no flux adjustments. Two ensemble members from HadCM3 GS simulations produce relatively large trends (–0.38 °C and –0.35 °C) for the period 1950–1999 that may be considered consistent with observations (–0.49 °C) after taking into account sampling uncertainty.

While results also indicate that GS forcing can explain much of the observed signal in MTG, results from HadCM2 indicate that volcanic aerosol forcing may also produce changes in MTG that are consistent with observations. This result supports suggestions from previous studies (Graf et al. 1998; Mao and Robock 1998; Kirchner et al. 1999) that changes in circulation and warming in the Northern Hemisphere high latitudes may be associated with volcanic eruptions.

Detection results for MTG again underline the limitations of using a single indicator of climate change in an attribution context. Considered alone and over short periods (less than 100 years), MTG and to a lesser extent global mean temperature provide ambiguous evidence for the attribution of climate change as they do not clearly differentiate between the effects of anthropogenic and natural forcing. In this respect, the combined normalised index provides an improved signal of climate change in much the same manner as spatial fingerprints, while being easier to analyse and interpret. For the CNI, only the GS response was found to have both consistent amplitude and temporal correlation with the observed index in all of the models except CSIRO Mk2 and ECHAM4 (both of which have relatively small GS

ensembles, with 1 and 2 member ensembles respectively). In addition, residual errors from regression of the GS forced responses of CNI are found to be consistent with climate noise. Considering multiple forcings simultaneously, the contribution of natural forcing factors to changes in CNI over the twentieth century are not significantly greater than changes due to internal climate variability. Amplitude scaling factors from CNI applied to global warming estimations are also found to be consistent with more-complex optimal fingerprint results and reinforce evidence that GS forcing makes a significant and dominant contribution to observed climate change during the last 100 years.

Acknowledgements This study was stimulated by our involvement in the preparation of the IPCC Third Assessment Report. We are grateful to Phil Jones for providing access to the observational data and to the IPCC Data Distribution Centre for providing access to additional climate model data, particularly the ECHAM4 data. Much of this research was carried out by Karl Braganza while he was supported by a graduate scholarship from the CRC for Southern Hemisphere Meteorology at Monash University. It has been completed while he has been funded as a research fellow through an ARC Discovery Grant at Monash University. Peter Stott and computer time for the HadCM2 and HadCM3 simulations was funded by the UK Department of Environment, Food and Rural Affairs under contract PECD 7/12/37. Simon Tett was funded by the UK GMR program.

References

Allen MR, Tett SFB (1999) Checking for model consistency in optimal fingerprinting. Clim Dyn 15: 419–434

Allen MR, Stott PA, Mitchell JFB, Schnur R, Delworth TL (2000) Quantifying the uncertainty in forecasts of anthropogenic climate change. Nature 407: 617–620

Braganza K, Karoly DJ, Hirst AC, Mann ME, Stott P, Stouffer J, Tett, SFB (2003) Simple indices of global climate variability and change: Part I, variability and correlation structure. Clim Dyn 20: 491–502

Collins M, Tett SFB, Cooper C (2001) The internal climate variability of HadCM3, a version of the Hadley Centre coupled model without flux adjustments. Clim Dyn 17: 61–81

Crowley TJ (2000) Causes of climate change over the past 1000 years. Science 289 270–277

Crowley TJ, Kim K-Y (1999) Modelling the temperature response to forced climate change over the last six centuries. Geophys Res Lett 26: 1901–1904

Cusack S, Slingo A, Edwards JM, Wild M (1998) The radiative impact of a simple aerosol climatology on the Hadley Centre GCM. QJR Meteorol Soc 124: 2517–2526

Delworth TL, Stouffer RJ, Dixon KW, Spelman MJ, Knutson TR, Broccoli AJ, Kushner PJ, Wetherald RT (2002) Review of simulations of climate variability and change with the GFDL R30 coupled climate model. Clim Dyn 19: 555–574

Dixon KW, Delworth Tl, Knutson TR, Spelman MJ, Stouffer RJ (2003) A Comparison of climate change simulations produced by two CFDL Coupled climate models. Global Planet change 37: 81–102

Edwards JM, Slingo A (1996) Studies with a flexible new radiation code. I: choosing a configuration for a large scale model. QJR Meteorol Soc 122: 689–719

Folland CK, Karl TR, Christy JR, Clarke RA, Gruza GV, Jouzel J, Mann ME, Oerlemans J, Salinger MJ, Wang S-W (2001) Observed climate variability and change. In Houghton, JT, Ding Y,Griggs DJ, Noguer M, van der Linden PJ, Dai X, Maskell K, Johnson CA (eds) Climate change 2001: The scientific basis, Contribution of Working Group 1 to the Third Assessment Report of the Intergovernmental Panel on Climate Change. Cambridge University Press, Cambridge, UK, pp 99–182

Free M, Robock A (1999) Global warming in the context of the Little Ice Age. J Geophys Res 104: 19,057–19,070

Gitelman AI, Risbey JR, Kass RE, Rosen RD (1997) Trends in the surface meridional temperature gradient. Geophys Res Lett 24: 1243–1246

Gitelman AI, Risbey JR, Kass RE, Rosen RD (1999) Sensitivity of a meridional temperature gradient index to latitudinal domain. J Geophys Res 104: 16,709–16,717

Graf H-F, Kirchner I, Schult I (1996) Modelling Mt. Pinatubo climate effects. NATO-ASI Series, vol 142, In: Fiocco G, Dua D (eds) The Mount Pinatubo Eruption, Springer, Berlin Heidelberg New York, pp 219–231

Gordon HB, O'Farrell SP (1997) Transient climate change in the CSIRO coupled model with dynamic sea-ice. Mon Weather Rev 125: 875–907

Gordon C, Cooper C, Senior CA, Banks HT, Gregory JM, Johns TC, Mitchell JFB, Wood RA (2000) The simulation of SST, sea ice extents and ocean heat transports in a version of the Hadley Centre coupled model without flux adjustments. Clim Dyn 16: 147–168

Hasselmann K (1993) Optimal fingerprints for the detection of time dependent climate change. J Clim 6: 1957–1971

Hegerl GC, Hasselmann K, Cubasch U, Mitchell JFB, Roeckner E, Voss R, Waszkewitz J (1997) Multi-fingerprint detection and attribution of greenhouse gas- and aerosol forced climate change. Clim Dyn 13: 613–634

Hirst AC (1999) The Southern Ocean response to global warming in the CSIRO coupled ocean-atmosphere model. Environ. Model Software: Spec Iss Modelling Global Climatic Change. 14: 227–242

Hirst AC, O'Farrell SP, Gordon HB, (2000) Comparison of a coupled ocean-atmosphere model with and without oceanic eddy-induced advection. 1. Ocean spin-up and control integrations. J Clim 13: 139–163

Hoyt DV, Schatten KH (1993) A discussion of plausible solar irradiance variations, 1700–1992. J Geophys Res 98: 18,895-18,905

Jain S, Lall U, Mann ME (1999) Seasonality and interannual variations of Northern Hemisphere temperature: equator to pole temperature gradient and land-ocean contrast. J Clim 12: 1086–1100

Johns TC (1996) A description of the Second Hadley Centre Coupled Model (HadCM2). Climate Research Technical Note 71, Hadley Centre, United Kingdom Meteorological Office, Bracknell Berkshire RG12 2SY, United Kingdom, pp 19

Johns TC, Carnell RE, Crossley JF, Gregory JM, Mitchell JFB, Senior CA, Tett SFB, Wood RA (1997) The second Hadley Centre coupled ocean-atmosphere GCM: model description, spin-up and validation. Clim Dyn 13: 103–134

Johns TC, Gregory JM, Stott PA, Mitchell JFB (2001) Correlations between patterns of 19th and 20th century surface temperature change and HadCM2 climate model ensembles. Geophys Res Lett 28: 1007–1010

Johns TC, Gregory JM, Ingram WJ, Johnson CE, Jones A, Lowe JA, Mitchell JFB, Roberts DL, Sexton DMH, Stevenson DS, Tett SFB, Woodage MJ (2003) Anthropogenic climate change for 1860 to 2100 simulated with HadCM3 model under updated emissions scenarios. Clim Dyn 20: 583–612

Jones PD (1995) Land surface temperatures- Is the network good enough? Clim Change 31: 545–558

Jones PD, New M, Parker DE, Martin S, Rigor IG (1999) Surface air temperature and its changes over the past 150 years. Rev Geophysics 37: 173–199

Karoly DJ, Braganza K (2001) Identifying global climate change using simple indices. Geophys Res Lett 28: 2205–2208

Kaufmann RK, Stern DI (1997) Evidence for human influence on climate from hemispheric temperature relations. Nature 388: 39–44

Kirchner I, Stenchikov GL, Graf H-F, Robock A, Antuna JC (1999) Climate model simulation of winter warming and summer cooling following the 1991 Mount Pinatubo volcanic eruption. J Geophys Res 104: 19,039–19,055

Lean J, Beer J, Bradley R (1995) Reconstruction of solar irradiance since 1610: Implications for climate change. Geophys Res Lett 22: 3195–3198

Manabe S, Stouffer RJ (1980) Sensitivity of a global climate model to an increase in the CO_2 concentration in the atmosphere. J Geophys Res 85: 5529–5554

Mann ME, Park J (1996) Greenhouse warming and changes in the seasonal cycle of temperature: Model versus observations. Geophys Res Lett 23: 1111–1114

Mao J, Robock A (1998) Surface air temperature simulations by AMIP general circulation models: volcanic and ENSO signals and systematic errors. J Clim 11: 1538–1552

McAvaney BJ, Covey C, Joussaume S, Kattsov V, Kitoh A, Ogana W, Pitman AJ, Weaver AJ, Wood RA, Zhao Z-C (2001) Model evaluation. In: Houghton JT, Ding Y, Griggs DJ, Noguer M, van der Linden PJ, Dai X, Maskell K, Johnson CA (eds) Climate change 2001: the scientific basis. Contribution of Working Group 1 to the Third Assessment Report of the Intergovernmental Panel on Climate Change. Cambridge University Press, Cambridge, UK, pp. 471–524

Meehl GA, Washington WM, Karl TM (1993) Low-frequency variability and CO_2 tanist climate change: Part 1. Time-averaged differences. Clim Dyn 8: 117–133

Mitchell JFB, Karoly DJ, Allen MR, Hegerl G, Zwiers F, Marengo J (2001) Detection of climate change and attribution of causes. In: Houghton JT et al. (eds) Climate change 2001: the scientific basis. Contribution of Working Group I to the Third Assessment Report of the Intergovernmental Panel on Climate Change. Cambridge University Press, Cambridge, UK, pp 695–738

Myers RH (1986) Classical and modern regression with applications. 2nd Edn. Duxbury Press, Belmont, Calfornia, pp 486

Oberhuber JM (1993) The OPYC ocean general circulation model. Techn Rep 7, Deutsches Klimarechenzentrum, Hamburg, Germany

Parker DE, Folland CK, Jackson M (1995) Marine surface temperature: Observed variations and data requirements. Clim Change 31: 559–600

Robock A (2000) Volcanic eruptions and climate. Rev Geophys 38: 191–219

Robock A, Free M (1995) Ice cores an index of global volcanism from 1850 to the present. J Geophys Res 100: 11,567–11,576

Roeckner E, Arpe K, Bengtsson L, Christoph M, Claussen M, Dümenil L, Esch M, Giorgetta M, Schlese U, Schulzweida U (1996a) The atmospheric general circulation model ECHAM4: Model description and simulation of present-day climate. MPI Report 218, Max-Planck-Institut für Meteorologie, Hamburg, Germany, pp 90

Roeckner E, Oberhuber JM, Bacher A, Christoph M, Kirchner I (1996b) ENSO variability and atmospheric response in a global coupled atmosphere-ocean GCM. Clim Dyn 12: 737–754

Santer BD, Wigley TML, Jones PD (1993) Correlation methods in fingerprint detection studies. Clim Dyn 8: 265–276

Santer BD, Taylor KE, Wigley TML, Johns TC, Jones PD, Karoly DJ, Mitchell JFB, Oort AH, Penner JE, Ramaswamy V, Schwarzkopf MD, Stouffer RJ, Tett SFB (1996) A search for human influences on the thermal structure in the atmosphere. Nature 382: 39–46

Sato M, Hansen JE, McCormick MP, Pollack J (1993) Stratospheric aerosol optical depths (1850–1990). J Geophys Res 98: 22,987–22,994

Shine KP, Forster PM (1999) The effects of human activity on radiative forcing of climate change: a review of recent developments. Global Planet Change 20: 205–225

Stott PA, Tett SFB (1998) Scale-dependent detection of climate change. J Clim 11: 3282–3294

Stott PA, Allen MR, Jones GS (2000a) Estimating signal amplitudes in optimal fingerprinting II: application to general circulation models. Hadley Centre Tech Note 20, Hadley Centre for Climate Prediction and Response, Meteorological Office, RG12 2SY UK

Stott PA, Tett SFB, Jones GS, Allen MR, Mitchell JFB, Jenkins GJ (2000b) External control of twentieth century temperature by natural and anthropogenic forcings. Science 290: 2133–2137

Stott PA, Tett SFB, Jones GS, Allen MR, Ingram WJ, Mitchell JFB (2001) Attribution of twentieth century temperature change to natural and anthropogenic Causes. Clim Dyn 17: 1–22

Tett SFB, Stott PA, Allen MR, Ingram WJ, Mitchell JFB (1999) Causes of twentieth century temperature change near the Earth's surface. Nature 399: 569–572

Tett SFB, Jones GS, Stott PA, Hill DC, Mitchell JFB, Allen MR, Ingram WJ, Johns TC, Johnson CE, Jones A, Roberts DL, Sexton DMH, Woodage MJ (2002) Estimation of natural and anthropogenic contributions to 20th century temperature change. J Geophys Res 107:doi 10.1029/2000JD000028

Thomson DJ (1995) The seasons, global temperature, precession and CO_2 Science 268: 59–68

Wigley TML, Barnett TP (1990) Detection of the greenhouse effect in the observations. In: Houghton JT, Jenkins GJ, Ephraums JJ (eds) Climate Change: The IPCC Scientific Assessment. Cambridge University Press, Cambridge, UK, pp 239–256

Wigley TML, Smith RL, Santer BD (1998) Anthropogenic influence on the autocorrelation structure of hemispheric-mean temperatures. Science 282: 1676–1679